Convergence of Time-Derivative Non-Adiabatic Couplings in Plane-Wave DFT Calculations

*Alva D. Dillon, Rebecca L.M. Gieseking**

Department of Chemistry, Brandeis University

415 South Street, Waltham, Massachusetts 02453

* Corresponding author: gieseking@brandeis.edu; (781)-736-2511

ABSTRACT

Accurate prediction of charge carrier relaxation rates is essential to design molecules and materials with the desired photochemical properties for applications like photocatalysis and solar energy conversion. Non-adiabatic molecular dynamics allows one to simulate the relaxation process of excited charge carriers. Plane-wave density functional theory (DFT) calculations make the time-derivative non-adiabatic couplings (TNACs) simple to compute because the basis is independent of the atomic positions. However, the effect of the kinetic energy cutoff for the plane-wave basis on the accuracy of the dynamics has not been studied. Here, we examine the effect of the kinetic energy cutoff on the TNACs and decay time scales for the prototypical model system of tetracene. These calculations show that the choice of kinetic energy cutoff can change the relaxation time by up to 30%. The relaxation times of states that have small TNACs to other states or are far from degenerate are more sensitive to the kinetic energy cutoff than those of states with large TNACs or near degeneracies. A kinetic energy cutoff of 60 Ry is sufficient for all states to reach qualitative agreement (absolute error < 10%) our reference decay time with our 110 Ry reference data, and a cutoff of 80 Ry is required for all states to reach quantitative agreement (absolute error < 2%).

KEYWORDS. Time Derivative Non-Adiabatic Coupling, Density Functional Theory, Time Dependent Kohn-Sham Theory, electron and hole relaxation, Plane-Wave Basis, Tetracene

1. Introduction

Understanding the photophysical properties of molecules[1–3] is essential to controlling important properties such as competition between radiative or non-radiative relaxation pathways,[4] photocatalytic activity,[5] and photoinduced charge separation.[6,7] These properties are dependent on the coupled nuclear and electronic dynamics following excitation by light; thus, accurate prediction of these dynamics is essential. Non-adiabatic molecular dynamics (NAMD) simulations describe the coupled evolution of the electronic and nuclear degrees of freedom during non-radiative relaxation of a photoexcited molecule.[8,9] The fewest switches surface hopping (FSSH) approach is a common method for simulating NAMD.[8–10] In the FSSH algorithm, the nuclei follow a classical trajectory, while the electrons are treated quantum mechanically; as the simulation proceeds, the electrons switch between electronic states with probabilities determined by the coupling between the electronic and nuclear degrees of freedom.[11] Details and extensions of the FSSH algorithm have been described thoroughly in many other papers.[12–17] The non-adiabatic coupling (NAC) vector used to compute the transition probability between states and how to scale atomic velocities after a state transition is computed as

$$d_{ij}(R) = \langle \psi_i(r;R) | \nabla_R | \psi_j(r;R) \rangle \quad (1)$$

where $d_{ij}(R)$ is the NAC between electronic states $\psi_i(r;R)$ and $\psi_j(r;R)$, which depend parametrically on the positions R of the nuclei, and ∇_R is the gradient of the nuclear positions.

FSSH simulations are computationally demanding even for small systems and are only feasible for large or condensed-phase systems with additional approximations that reduce the computational cost.[18] First, approximations are often made to the nuclear dynamics. If the ground-

state and excited-state potential energy surfaces are similar, the classical path approximation can be used without substantially changing the nuclear dynamics.[9,11,19,20] In the classical path approximation, the back-reaction of the excited electrons on the nuclei is neglected, and a classical nuclear trajectory that is independent of the electron dynamics is used. Thus, a ground-state trajectory can be pre-computed, and the NACs can be pre-computed based on a series of known geometries. This approximation is often suitable for the excited-state dynamics of systems with up to hundreds of atoms where an electronic excitation does not significantly change the overall electron density,[21] including molecular complexes,[21] solids,[8] and condensed phase systems.[11]

In addition, approximations must be made to the electronic states. Although multi-reference or configuration-interaction-based approaches typically produce the most accurate NACs,[22,23] they are often too computationally expensive. For large systems, time-dependent density functional theory (TDDFT) may also be too computationally expensive to be tractable for a large number of time steps.[18] Approaches based on time-dependent Kohn-Sham (TD-KS) theory also have a reduced computational cost.[18,24] TD-KS theory uses the single particle approximation to model electronic states either as single Kohn-Sham orbitals or as Slater determinants involving a excitation from one Kohn-Sham orbital to another.[11,25,26] This approach has produced results in agreement with TDDFT for systems where the single-particle approximation is reasonable, including organic-inorganic complexes, quantum dots, and some small molecules.[25]

When using the classical path approximation and TD-KS orbitals, the formula for the NACs[27] can be simplified to the time-derivative NACs (TNACs) between the electronic states at consecutive time steps using the Hammes-Schiffer[28] formulation:

$$d_{ij} = \frac{\langle \phi_i(t) | \phi_j(t+\Delta t) \rangle - \langle \phi_i(t+\Delta t) | \phi_j(t) \rangle}{2 \cdot \Delta t} \quad (2)$$

where ϕ_i and ϕ_j are Kohn-Sham orbitals at consecutive time points t and $t + \Delta t$. In the Slater determinant (SD) basis, the time overlaps are computed using the Lowdin formula:[29,30]

$$\langle \varphi_p(t) | \varphi_q(t+\Delta t) \rangle = \det S[pq] \quad (3)$$

where $S[pq]$ is the matrix of the time overlaps between the occupied molecular orbitals in the Slater determinants $\varphi_p(t)$ and $\varphi_q(t + \Delta t)$.

Using these approximations to compute the TNACs, several factors can strongly affect the accuracy of the TNACs and thus of the decay time scales. The quality of the computed TNACs depends strongly on the level of theory.[11,31] For example, Generalized Gradient Approximation (GGA) functionals are well-known to underestimate band gaps; thus, it is unsurprising that the GGA functional PBE predicts TNACs an order of magnitude larger than those computed using hybrid functionals with exact exchange.[32,33] The accuracy of PBE can be improved by using an electron self-energy correction to correct the band gap.[34] Aside from the functional used to compute the TNACs, the length of the trajectory and the average magnitude of the TNACs over the trajectory can also affect the accuracy of the decay time scales.[35]

A factor that has been largely neglected in understanding the accuracy of TNACs is the role of the basis set. TNACs are often computed using plane-wave basis sets because of the simplicity of computing overlaps of these functions; in these calculations, the molecular orbitals are described by a plane-wave expansion:[36]

$$\psi_{i,k}(r) = \sum_G \psi_{i,k}(G) \frac{e^{i(k+G)r}}{\sqrt{\Omega}} \quad (4)$$

where the i is the Kohn-Sham orbital index, k is the Bloch vector, G are the reciprocal lattice vectors, and Ω is the volume of the periodic box used to describe our system. Typically, all plane waves with energies below a given kinetic energy cutoff are included in this expansion; the kinetic energy cutoff is often chosen by converging the total energy of the system with respect to the kinetic energy cutoff. Since a higher kinetic energy cutoff yields a more accurate description of the molecular orbitals, the TNACs will depend on the kinetic energy cutoff. However, to our knowledge it is not known whether the cutoff that converges total energy is sufficient to provide converged TNACs. In previous studies, the kinetic energy cutoff is often provided,[11,37–45] while other studies report using a converged plane wave basis.[21,46–48]

Here, we examine the dependence of the TNACs and excited-state dynamics on the kinetic energy cutoff by performing FSSH simulations using the classical path approximation with TD-KS electronic states. We use tetracene as a prototypical model system: its rigid structure and relatively constant electron density upon excitation make is suitable for the classical path approximation, and its electronic structure is well known.[49,50] Our results show that the TNACs converge qualitatively (absolute error < 10%) with our reference TNACs at a kinetic energy cutoff of 60 Ry. To achieve quantitative (absolute error < 2%) agreement with our reference data, a kinetic energy cutoff of 80 Ry was required. Our results show that the decay dynamics are much less sensitive to the kinetic energy cutoff than to previously studied factors like the choice of DFT functional.

2. Computational Methods

The geometry of tetracene was optimized at the PBE level[51] within a box with dimensions 4.5 x 4.5 x 4.5 nm and a kinetic energy cutoff of 40 Ry. Starting from this geometry, the ground-state nuclear trajectory was computed at the same level of theory and kinetic energy cutoff for 2400 steps with a time step of 1 fs, resulting in a 2.4 ps trajectory. The Verlet algorithm was used to integrate Newton's equations of motion, and the atomic velocities were adjusted with an Anderson thermostat to maintain a temperature of 300 K.

To ensure that the FSSH simulations were performed using equilibrated geometries, the TNACs were computed using only time steps from step 300 until the end of the nuclear trajectory. For each time step in this range, the electronic structure was computed using the PBE functional[52] with kinetic energy cutoffs ranging from 20 to 110 Ry in steps of 10 Ry. All calculations were performed using norm-conserving pseudopotentials[53] within the Quantum Espresso software package.[54]

The TNACs were computed for all pairs of Slater determinants within a basis set from HOMO-2 to LUMO+2, using phase corrections to ensure consistency of the molecular orbitals at different time steps.[55] The excited-state dynamics were computed using the FSSH algorithm with the transition probabilities rescaled by a Boltzmann factor.[11] Following the truncation of the trajectory, an initial starting point for the NAMD trajectory was chosen every 20 time steps from 300-1900 fs time step for a total of 70 starting points and propagated for 500 fs, and 2500 stochastic trajectories for the FSSH algorithm for each starting point. We chose to do 2500 electron

trajectories, at least 10 times what is typical in NAMD studies, for each starting point to average out the stochastic contribution to provide a precise estimate of the decay time scales based on the TNACs. The population of the system remaining in the initial state was fit to a single exponential decay:

$$f(t) = ae^{-\lambda_i t}$$

where a is the initial population of state i and λ_i is the decay rate. Based on this fit, the relaxation time was computed as $\tau_i = \frac{1}{\lambda_i}$. To confirm that the stochastic contributions to the relaxation times are negligible the standard deviation (σ) of the relaxation times from the 5 FSSH simulations is calculated as

$$\sigma = \sqrt{\frac{\sum(\tau_i - \bar{\tau})^2}{5}}$$

where τ_i is the relaxation time of the initial state from the i^{th} simulation and $\bar{\tau}$ is the average relaxation time from the 5 FSSH simulations. The percent error for the relaxation times computed with lower kinetic energy cutoffs are computed as

$$\%\, Error = \frac{\bar{\tau}_k - \bar{\tau}_{110\ Ry}}{\bar{\tau}_{110\ Ry}} \times 100\%$$

where $\bar{\tau}_k$ is the average relaxation time using kinetic energy cutoff k and $\bar{\tau}_{110\ Ry}$ is the average of the reference relaxation times computed with a 110 Ry kinetic energy cutoff. TNACs and FSSH simulations were performed using the methodology development code Libra.[56]

3. Results and Discussion

The overall goal of this study is to examine the effect of the kinetic energy cutoff on TNACs and decay time scales by comparing the results for a series of kinetic energy cutoffs to reference data computed with a cutoff of 110 Ry. We selected tetracene (Figure 1) as a model system because its rigid structure makes the classical path approximation a suitable choice. The optical properties and excited state dynamics of tetracene have been reported in several studies of polycyclic aromatic hydrocarbons (PAHs).[49,50]

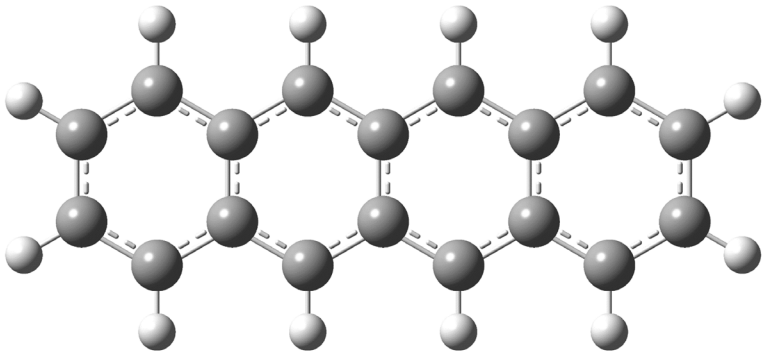

Figure 1: Chemical structure of tetracene.

We focus on an active space from the HOMO-2 to LUMO+2 Kohn-Sham molecular orbitals (MOs). Within this range, tetracene has two pairs of nearly degenerate MOs: (1) HOMO-1 and HOMO-2, and (2) LUMO+1 and LUMO+2. Using the MOs within this range, we generate a Slater determinant basis including all possible single excitations of the alpha electrons, plus the ground state. The energies of the SDs are calculated as the sum of the energies of the occupied Kohn-Sham in each SD as implemented in Libra:

$$E_{SD_{occ}} = \sum_{i \ni occ_{KS}} \varepsilon_i \tag{1}$$

where ε_i is the orbital energy. The near degeneracies in the MOs result in two groups of SDs with nearly degenerate energies (Figure 2a). The first set is around -20.7 eV, approximately 3 eV above the ground-state energy, and the second set is around -19.2 eV, around 4.5 eV above the ground state. The nearly degenerate pairs of SDs have TNACs that are on average much larger than the TNACs between any non-degenerate pair of SDs (Figure 2a). As expected, the energies of the SDs fluctuate but do not dramatically change throughout the course of the 2400 fs ground-state trajectory.

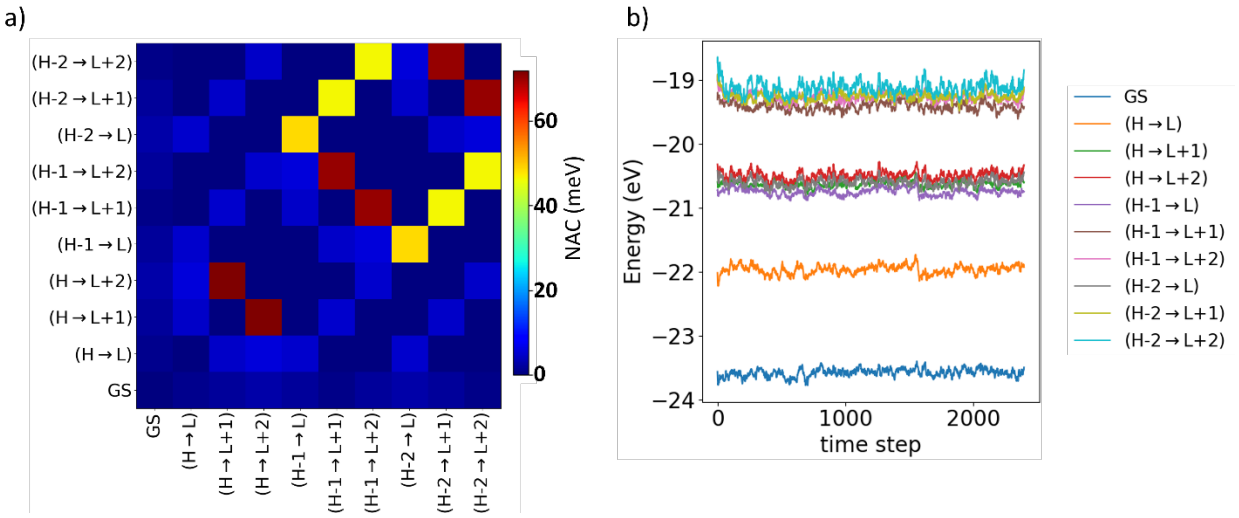

Figure 2: a) Average TNACs over the geometric trajectory and b) energy of Slater determinants over time calculated using the PBE functional with 110 Ry kinetic energy cutoff.

We now examine the effect of the kinetic energy cutoff. As discussed in the Introduction, convergence of total energy is commonly used as a proxy for convergence of the dynamics. For this system, the total energy of the optimized geometry follows the expected exponential-like decrease with increasing kinetic energy cutoff, converging to within 0.003 Ry of its reference value

(110 Ry cutoff) at a kinetic energy cutoff of 100 Ry (Figure 3a). However, this higher accuracy comes at a tradeoff of higher computational cost: as the cutoff increases from 20 to 110 Ry, the CPU time for a single-point energy calculation on a single geometry increases from 5 to 35 minutes, shown in Figure 3b. Since a single geometric trajectory long enough for NAMD simulations typically contains thousands of geometries, small differences in computational time for each geometry add up over the course of a trajectory.

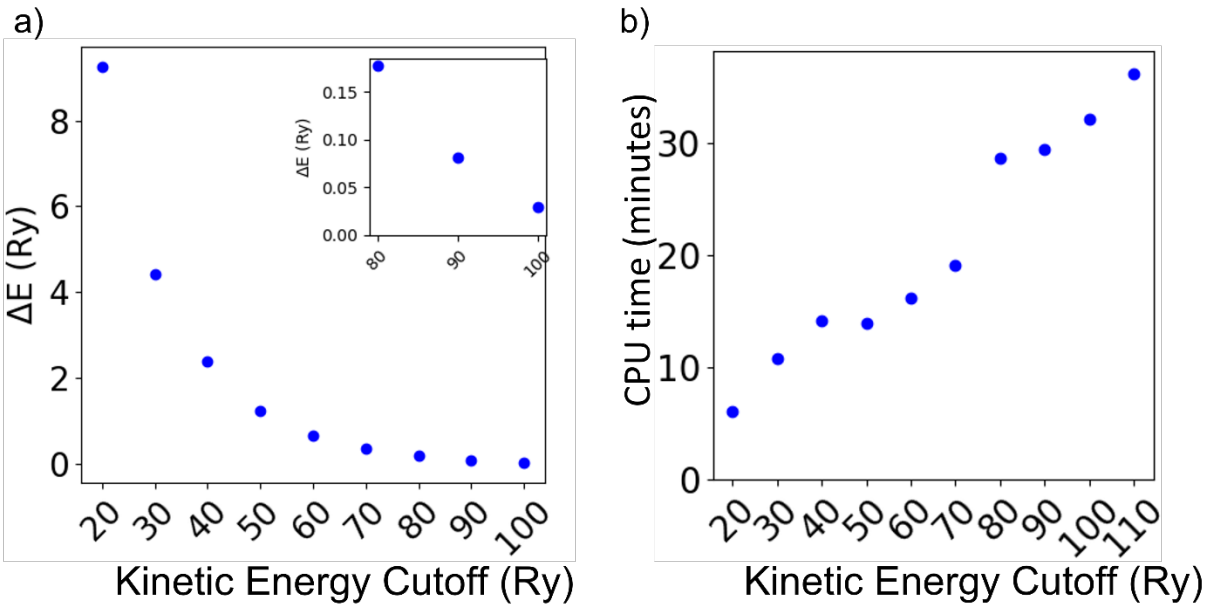

Figure 3:a) Total energy convergence, zoom in on total energy convergence (inset) b) Plot of CPU time for single point energy calculation of same tetracene geometry with different kinetic energy cutoffs.

3.1. TNACs in Slater determinant basis

Although checking convergence of the total energy and electronic states with respect to the kinetic energy cutoff is relatively common in NAMD studies,[32,57,58] it is not known to date whether this approach of choosing a kinetic energy cutoff is sufficient to converge the TNACs. Since the TNACs determine the hopping probabilities, differences in the TNACs between different kinetic energy cutoffs may lead to differences in the dynamics. For all kinetic energy cutoffs, we use the same nuclear trajectory; thus, any difference in the TNACs is due only to the change in cutoff.

In a TDDFT framework, the first strongly absorbing state of tetracene is a linear combination of multiple SDs.[49,50] However, since our focus is on understanding how the kinetic energy cutoff changes the TNACs in a molecule, we focus on the TNACs between SDs; the full TDDFT excited states are too computationally expensive to be practical, particularly for the higher kinetic energy cutoffs. We focus first on the TNAC between the $(\mathrm{HOMO}-1 \rightarrow \mathrm{LUMO}+1)$ and $(\mathrm{HOMO}-1 \rightarrow \mathrm{LUMO}+2)$ SDs, which has one of the largest TNACs on average. To visualize the convergence of the TNACs, we use correlation plots between the TNACs calculated using different kinetic energy cutoffs (Figure 4). For different geometric pairs within this trajectory, the value of this TNAC in our reference data (kinetic energy cutoff of 110 Ry) ranges from 0.08 meV to 634.98 meV, with a mean of 70.26 meV. At the lowest kinetic energy cutoff of 20 Ry, the average value of this TNAC is 75.27 meV, in reasonable agreement with the reference value. However, there is significant scatter between the TNACs computed at 20 Ry and the reference data, with some geometry pairs having deviations larger than 300 meV. Since this cutoff is far below what is typically used in plane-wave calculations, these large deviations are unsurprising.

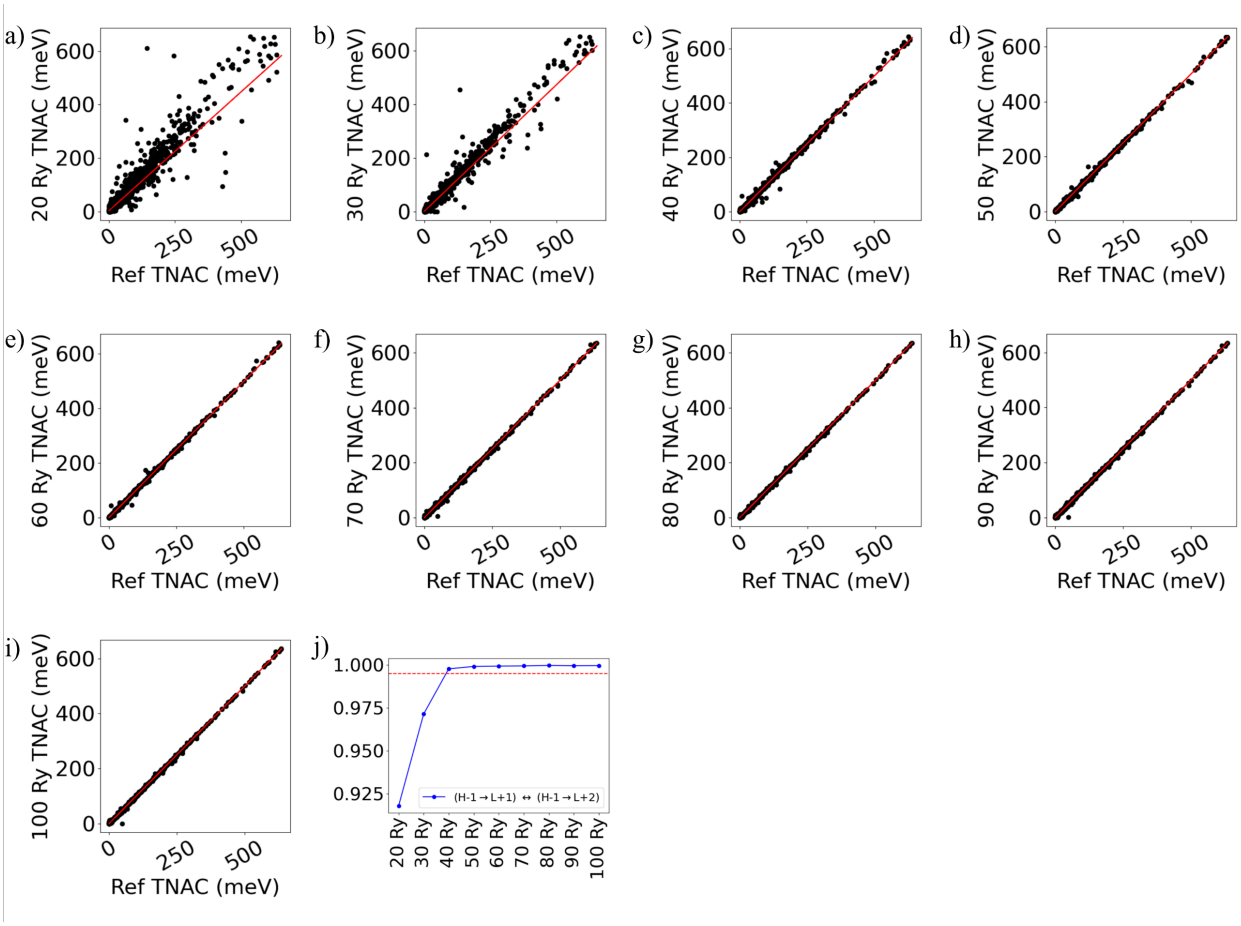

Figure 4: Correlation plots for TNAC between $(HOMO-1 \rightarrow LUMO+1)$ *and* $(HOMO-1 \rightarrow LUMO+2)$ *Slater determinants comparing TNACs at different kinetic energy cutoffs to the 110 Ry benchmark data. TNACs from the 110 Ry trajectory are shown on x-axis and kinetic energy cutoffs for a) 20 Ry, b) 30 Ry, c) 40 Ry, d) 50 Ry, e) 60 Ry, f) 70 Ry, g) 80 Ry, h) 90 Ry, and i) 100 Ry on the y-axis. The final plot j) shows the collection of* R^2 *values from the correlation plots in a) - i).*

As the kinetic energy cutoff increases, the agreement between the TNACs and the reference data improves, as the points cluster closer to the line of best fit and the number of outliers decreases (Figure 4). We can quantify this agreement using the slope, intercept, and R^2 value for the line of best fit; perfect correlation implies a slope of 1, intercept of 0, and R^2 value of 1. In practice, for all Slater determinant pairs, all three of these values generally approach their ideal values as the kinetic energy cutoff increases. That improvement is not always monotonic; for example, an increase in cutoff from 50 to 60 Ry (Figure 4 d,e) leads to an increase in the intercept and a change in slope from slightly less than 1 to slightly more than 1. We focus on R^2 to determine the level of agreement between the TNACs from a particular cutoff and our reference data, shown in Figure 4j. The red dotted line in Figure 4j is at 0.995, marking a 0.5% error threshold from a perfectly correlated system, where at or above this point we consider the TNAC to be converged. For this particular TNAC, the R^2 value increases sharply as the kinetic energy cutoff increases from 20 to 40 Ry and passes the convergence threshold at 40 Ry; for larger kinetic energy cutoffs, R^2 remains very close to 1.

We now examine the remaining TNACs within our SD basis to examine their convergence with the kinetic energy cutoff. We focus only on the evolution of R^2 with kinetic energy cutoff; correlation plots for these TNACs are included in the supporting information (Figures S1-S20). Within the basis of 10 SD, there are a total of 45 unique unordered pairs with different TNACs, with average values ranging from 0.002 meV to 71 meV (Figure 2a). Since larger TNACs correspond to more probable transitions, we focus here on the 20 pairs with TNACs that average at least 2 meV in our reference data. Most of the SD pairs with average TNACs smaller than this cutoff involve transitions in both the occupied and the unoccupied MOs (for example, (HOMO →

LUMO) and (HOMO − 1 → LUMO + 1)), so it is unsurprising that their coupling is very small. We consider a TNAC converged if its correlation with the reference data yields $R^2 \geq 0.995$.

We focus first on the TNACs with the largest average magnitude (40 – 75 meV), shown in Figure 2a, which correspond to the red and yellow squares in Figure 1a. All these TNACs are between states that are nearly degenerate because each transition involves a change in MOs within a nearly degenerate pair: either LUMO+1↔LUMO+2 or HOMO-1↔HOMO-2. These TNACs follow two distinct convergence patterns. The three TNACs involving LUMO+1↔LUMO+2 transitions all have R^2 values around 0.92 for the lowest kinetic energy cutoff of 20 Ry, and R^2 increases somewhat at 30 Ry before reaching the convergence threshold of > 0.995 at a cutoff of 40 Ry; the SD pair shown in Figure 4 was one of these three TNACs. In contrast, the three TNACs involving HOMO-1↔HOMO-2 transitions have their lowest R^2 values at a 30 Ry cutoff and reach the convergence threshold of at a cutoff of 50 Ry. For all six of these TNACs, R^2 is above the convergence threshold at all kinetic energy cutoffs ≥ 50 Ry. Interestingly, the large TNACs have much smaller values of R^2 for the lowest two kinetic energy cutoffs than the smaller TNACs shown Figure 5b-c. This suggests that nearly degenerate orbital pairs may be more sensitive to changes in the basis set than non-degenerate orbitals. Since the largest TNACs also lead to the fastest decay time scales, obtaining reasonably accurate values for these TNACs is particularly important.

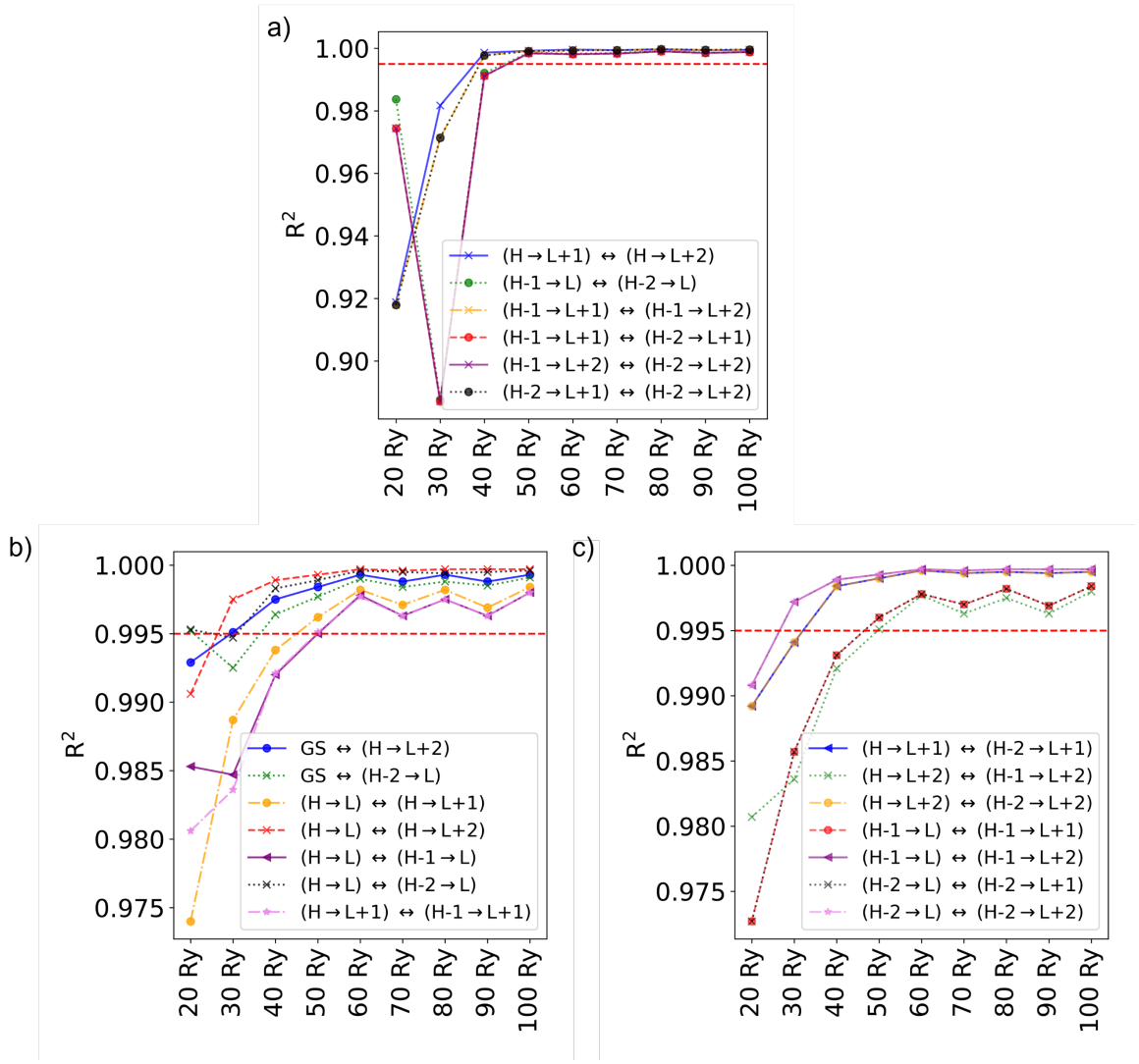

Figure 5: Correlation coefficients from correlation plots of TNACs computed with different kinetic energy cutoffs in the Slater determinant basis. Figure a) shows TNACs that have a large magnitude (red or yellow squares in figure 2 a). Figures b) and c) show TNACs with smaller magnitudes (light blue squares in figure 2 a). All TNACs in a) b) and c) are ordered by their matrix index, example in figure 2 a (origin is bottom left corner).

We now examine the TNACs with smaller average magnitudes (2 – 6 meV), shown in Figure 5b-c; this molecule has no TNACs with average values between 6 meV and 40 meV. The three TNACs that involve a transition between the LUMO and LUMO+1 all have R^2 values around 0.975 for the lowest kinetic energy cutoff of 20 Ry, and R^2 increases until reaching the convergence threshold at a cutoff of 50 Ry; at larger kinetic energy cutoffs, the R^2 values of these TNACs oscillate above the convergence threshold. The three TNACs involving a HOMO↔HOMO-1 transition similarly reach convergence at 50 Ry but oscillate above the convergence threshold at larger kinetic energy cutoffs. In contrast, the three TNACs involving HOMO↔HOMO-2 transitions converge at 40 Ry, and the three TNACs involving a transition from LUMO↔LUMO+2 converge at 30 Ry; all of these TNACs have larger and more consistent R^2 values than the previous sets. A few of these TNACs are above the convergence threshold at 20 Ry but dip below the convergence threshold at 30 Ry. Because of the variation in the cutoff required to reach convergence for different TNACs, an intermediate kinetic energy cutoff may be sufficient to obtain accurate results for some but not all of the TNACs. However, since the convergence threshold we selected is somewhat arbitrary, convergence of the TNACs based on this threshold does not necessarily imply that the relaxation dynamics are converged to the same level. We will examine the relationship between convergence of TNACs and convergence of dynamics in the following section.

3.2. Fewest Switches Surface Hopping Dynamics Slater Determinant Basis

After examining the effect of the kinetic energy cutoff on the TNACs, we now turn to the effect of this cutoff on the relaxation times. This will give insight into how tightly converged the TNACs

need to be to obtain quantitatively or qualitatively converged relaxation times. To ensure that the variation in our relaxation times is due to differences in the TNACs and not on the stochastic contributions of the surface hopping algorithm, our relaxation times are computed based on 5 independent FSSH simulations, each using 2500 stochastic realizations of our FSSH simulations at 70 different start times. The standard deviation of the relaxation time out of each initial state is less than 5% of the relaxation time, and in most cases less than 1%, confirming that the number of trajectories is large enough to fully converge the relaxation time. As before, we use the average relaxation time produced from the FSSH simulation using the 110 Ry TNACs as a benchmark.

Several examples of the change in population over time from various initial states are shown in Figure 6. When the initial state is the (HOMO→LUMO+1) SD, the relaxation time is relatively long at nearly 800 fs, and the population transfers primarily to the (HOMO→LUMO) and ground state SDs. This slow decay is unsurprising since (HOMO→LUMO+1) has small TNACs to both the (HOMO→LUMO) and ground state SDs (Figure 2). The (HOMO-2 →LUMO) SD decays much more quickly to the (HOMO-1→LUMO) SD because the TNAC between those SDs is much larger. Following population transfer to (HOMO-1→LUMO), the system decays more slowly into (HOMO→LUMO) and the ground state. The (HOMO-2→LUMO+2) SD has relatively large TNACs to multiple SDs, resulting in multiple decay pathways involving fast population transfer to the (HOMO-2→LUMO+1), (HOMO-1→LUMO+2), and (HOMO-1→LUMO+1) SDs and slower decay into lower-energy SDs. The decay pathways for the other initial SDs are shown in the SI.

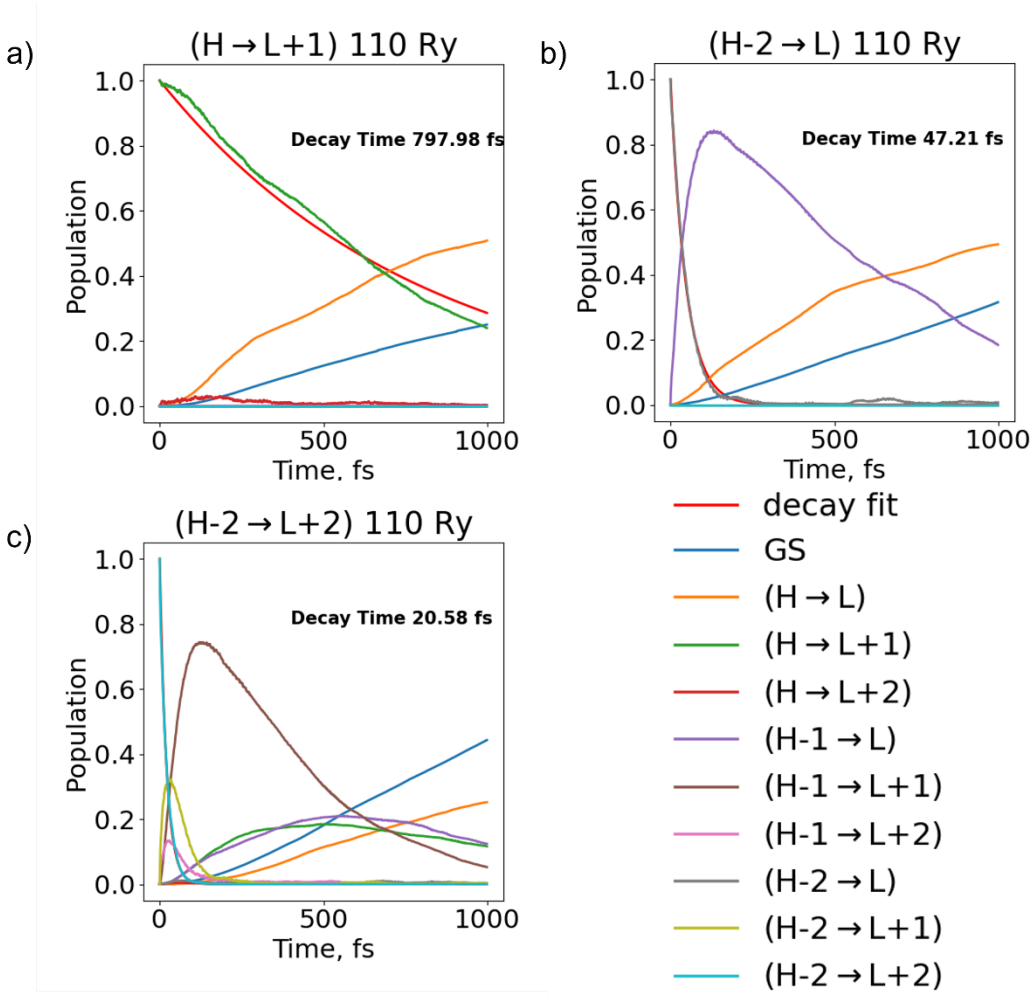

Figure 6: Time evolution of the population for the a) (HOMO →LUMO+1), b) (HOMO-2→LUMO), and c) (HOMO-2→LUMO+2) initial states calculated with 110 Ry kinetic energy cutoff.

To evaluate the convergence of the dynamics, we focus solely on the relaxation time out of the initial state; the relative importance of the different decay pathways for each initial state is largely consistent for all kinetic energy cutoffs. We do not consider the (HOMO→LUMO) SD as an initial state because the ground state is the only energetically accessible SD for decay, and the TNAC between the ground state and excited SDs is not well justified for a singly excited method. For all

initial states, the absolute value of the % error for all kinetic energy cutoffs is < 30%, meaning that even the smallest kinetic energy cutoffs consistently give qualitative agreement with the reference data. This is unsurprising given that the kinetic energy cutoff has a relatively small effect on the average TNAC over the course of the trajectory, even if the TNAC at each particular time step may have significant error. To make consistent comparisons, we consider the relaxation time to be semi-quantitatively converged when the absolute value of the % error is < 10% and quantitatively converged when the absolute value of the % error is < 2%.

Among the higher-energy initial states, the SDs that only involve molecular orbitals within an active space from HOMO-1 to LUMO+1 have decay times between 400 and 1000 fs (Figure 7a). The three initial SDs have small differences in the convergence pattern of the dynamics with kinetic energy cutoff. The relaxation time of the HOMO→LUMO+1 SD reaches semi-quantitative convergence (< 10% error) at 40 Ry, whereas the HOMO-1→LUMO and HOMO-1→LUMO+1 SDs do not reach semi-quantitative convergence until kinetic energy cutoffs of 70 Ry and 60 Ry, respectively. All three of these initial SDs reach quantitative convergence (< 2% error) of the relaxation times at kinetic energy cutoffs of 70-80 Ry. For these three initial states, the TNACs involved in the main decay pathways all converged at 50 Ry or lower. This suggests that the TNACs must converge to a tighter cutoff than the 0.995 value used in the previous section before quantitative convergence of the decay dynamics is achieved.

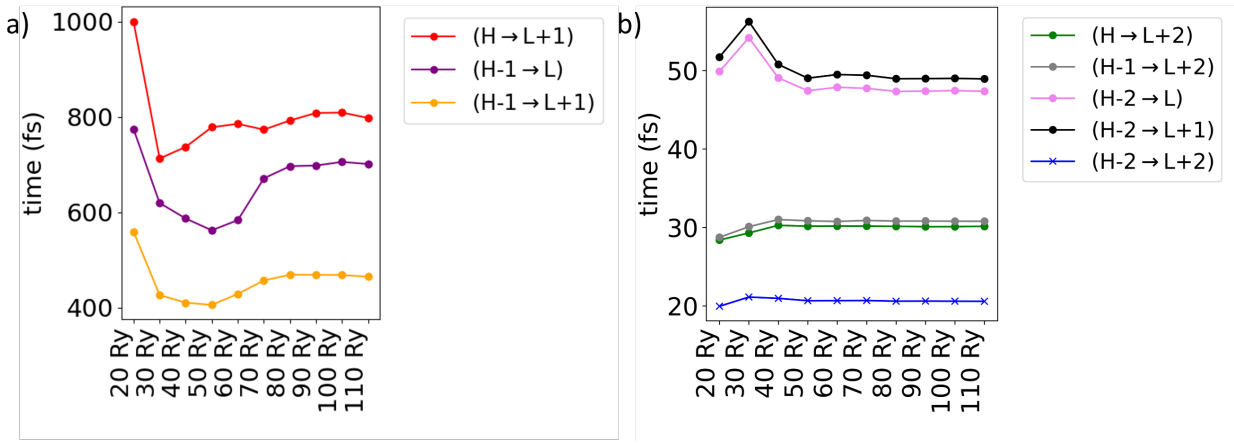

Figure 7: Simulated decay times from five FSSH simulations, with 2500 stochastic realiazations, 70 initial starting points, over 500, 1 fs time steps to obtain error bars for decay times. Error bars are present for all traces.

For all SDs that involve either HOMO-2 or LUMO+2 (Figure 7b), the relaxation times are below 60 fs; the fast decay is consistent with the much larger magnitudes of the TNACs and the near-degeneracy of the MOs. The HOMO-2→LUMO+1 and HOMO-2→LUMO SDs achieve semi-quantitative convergence at a kinetic energy cutoff of 40 Ry and quantitative convergence at 50 Ry. For both states, the main initial decay pathway involves a transition between HOMO-2 and HOMO-1; as was shown previously, the TNACs involving this transition have particularly large errors at 30 Ry. In contrast, all three SDs involving LUMO+2 are semi-quantitatively converged for the smallest kinetic energy cutoff of 20 Ry and reach quantitative convergence at 40 Ry. This semi-quantitative convergence occurs despite the fact that the TNACs for the relevant decay pathways have much smaller R^2 values at 20 and 30 Ry than most of the smaller TNACs. This

suggests that achieving tight convergence of the TNACs may be less important for states that decay quickly than for states with slower decay.

4. Conclusions

FSSH simulations are a powerful tool to explore the photophysical properties of molecules and materials. Because of the high computational expense of these simulations, many approximations must be made when computing the TNACs. Here, we examined the effect of the kinetic energy cutoff on the TNACs and the resulting decay times for a prototypical model system. Higher kinetic energy cutoffs give a more complete description of the orbitals and thus are expected to yield more accurate TNACs.

For our model system, all TNACs in the SD basis converge to an R^2 value > 0.995 by a kinetic energy cutoff of 50 Ry, and many TNACs converge as early as 30-40 Ry. Interestingly, the largest TNACs are the farthest from this convergence threshold at very small kinetic energy cutoffs (20-30 Ry). However, even when R^2 is relatively small, the average TNAC across the trajectory is in good agreement with the high kinetic energy cutoff reference data.

The choice of kinetic energy cutoff does not significantly change the decay pathway for each initial state. However, the kinetic energy cutoff does have some effect on the time scale of the decay. Initial states with large energy gaps to neighboring lower-energy states and smaller TNACs have slower decay times that depend more strongly on the kinetic energy cutoff. Even for the initial states with the largest variation in decay times, the smallest kinetic energy cutoff of 20 Ry yields

decay times within 30% of the reference value. Achieving quantitative convergence (< 2% error) of the decay times relative to the reference data requires kinetic energy cutoffs as high as 80 Ry for a few initial states, which is much higher than the cutoff that was required to obtain convergence of the TNACs. In contrast, the initial states that are strongly coupled to lower-energy states showed much less dependence of their decay time scales on the kinetic energy cutoff and reached quantitative convergence at 50 Ry or lower.

These results suggest that the FSSH algorithm using TNACs is overall quite robust to the kinetic energy cutoff. Even at the lowest kinetic energy cutoff of 20 Ry, which is far lower than is used in practice, all of the initial states we examined had decay times within 30% of their converged values. Since the largest errors in decay time scales were seen for the lowest-energy initial states with the fewest possible decay pathways, we expect this result to also hold for higher-energy initial states than those included in our basis set. Given that the choice of functional can change TNACs by up to an order of magnitude, the magnitude of changes with kinetic energy cutoff is surprisingly small. This suggests that one has a great deal of flexibility in choosing an appropriate kinetic energy cutoff. A larger cutoff is more important for initial states that are energetically isolated or weakly coupled to other states, or if one wants results that are quantitatively converged with respect to the kinetic energy cutoff. Given the number of other approximations inherent in FSSH simulations, the qualitative convergence that can be achieved with small kinetic energy cutoffs is likely adequate for many applications, and the lower computational cost of a small cutoff facilitates application of FSSH to a wide variety of chemical systems.

Acknowledgments

The authors would like to thank Alexey Akimov, Brendan Smith, and Mohammad Shakiba for helpful discussions. This project was funded by ACS Petroleum Research Fund Award No. ACS PRF 62073-DNI6. Computational work was performed on the Brandeis HPCC, which is partially supported by the NSF through DMR-MRSEC 2011846 and OAC-1920147.

References

[1] M.V. Bobo, J.J. Kuchta, and A.K. Vannucci, "Recent advancements in the development of molecular organic photocatalysts," Org Biomol Chem **19**(22), 4816–4834 (2021).

[2] C. Wu, N. Corrigan, C.H. Lim, W. Liu, G. Miyake, and C. Boyer, "Rational Design of Photocatalysts for Controlled Polymerization: Effect of Structures on Photocatalytic Activities," Chem Rev **122**(6), 5476–5518 (2022).

[3] G. Joshi, A.Q. Mir, A. Layek, A. Ali, S.T. Aziz, S. Khatua, and A. Dutta, "Plasmon-Based Small-Molecule Activation: A New Dawn in the Field of Solar-Driven Chemical Transformation," ACS Catal **12**(2), 1052–1067 (2022).

[4] C. Song, Z. Wang, Z. Yin, D. Xiao, and D. Ma, "Principles and applications of photothermal catalysis," Chem Catalysis **2**(1), 52–83 (2022).

[5] Z. Zhang, G. Yi, P. Li, X. Zhang, H. Fan, Y. Zhang, X. Wang, and C. Zhang, "A minireview on doped carbon dots for photocatalytic and electrocatalytic applications," Nanoscale **12**(26), 13899–13906 (2020).

[6] M. Schulz, N. Hagmeyer, F. Wehmeyer, G. Lowe, M. Rosenkranz, B. Seidler, A. Popov, C. Streb, J.G. Vos, and B. Dietzek, "Photoinduced Charge Accumulation and Prolonged

Multielectron Storage for the Separation of Light and Dark Reaction," J Am Chem Soc **142**(37), 15722–15728 (2020).

[7] R. Yanagi, T. Zhao, D. Solanki, Z. Pan, and S. Hu, "Charge Separation in Photocatalysts: Mechanisms, Physical Parameters, and Design Principles," ACS Energy Lett **7**(1), 432–452 (2022).

[8] O. V. Prezhdo, "Modeling Non-adiabatic Dynamics in Nanoscale and Condensed Matter Systems," Acc Chem Res **54**(23), 4239–4249 (2021).

[9] T.R. Nelson, A.J. White, J.A. Bjorgaard, A.E. Sifain, Y. Zhang, B. Nebgen, S. Fernandez-Alberti, D. Mozyrsky, A.E. Roitberg, and S. Tretiak, "Non-adiabatic Excited-State Molecular Dynamics: Theory and Applications for Modeling Photophysics in Extended Molecular Materials," Chem Rev **120**(4), 2215–2287 (2020).

[10] M. Barbatti, and R. Crespo-Otero, "Surface hopping dynamics with DFT excited states," Top Curr Chem **368**, 415–444 (2015).

[11] A. v. Akimov, and O. v. Prezhdo, "The PYXAID program for non-adiabatic molecular dynamics in condensed matter systems," J Chem Theory Comput **9**(11), 4959–4972 (2013).

[12] L. Wang, D. Trivedi, and O. v. Prezhdo, "Global flux surface hopping approach for mixed quantum-classical dynamics," J Chem Theory Comput **10**(9), 3598–3605 (2014).

[13] L. Wang, A. Akimov, and O. v. Prezhdo, "Recent Progress in Surface Hopping: 2011-2015," Journal of Physical Chemistry Letters **7**(11), 2100–2112 (2016).

[14] J. Qiu, X. Bai, and L. Wang, "Crossing Classified and Corrected Fewest Switches Surface Hopping," Journal of Physical Chemistry Letters **9**(15), 4319–4325 (2018).

[15] L. Wang, A.E. Sifain, and O. v. Prezhdo, "Fewest Switches Surface Hopping in Liouville Space," Journal of Physical Chemistry Letters **6**(19), 3827–3833 (2015).

[16] C.C. Martens, "Classical and nonclassical effects in surface hopping methodology for simulating coupled electronic-nuclear dynamics," Faraday Discuss **221**(0), 449–477 (2019).

[17] B. Smith, and A. v. Akimov, "A comparative analysis of surface hopping acceptance and decoherence algorithms within the neglect of back-reaction approximation," J Chem Phys **151**(12), 124107 (2019).

[18] M. Barbatti, and R. Crespo-Otero, "Surface hopping dynamics with DFT excited states," Top Curr Chem **368**, 415–444 (2015).

[19] S.A. Fischer, B.F. Habenicht, A.B. Madrid, W.R. Duncan, and O. v Prezhdo, "Molecular dynamics with electronic transitions," J Chem Phys **134**, 24102 (2011).

[20] S.D. Augustin, and H. Rabitz, "The classical path approximation in time-dependent quantum collision theory," J Chem Phys **69**(9), 4195 (2008).

[21] S.A. Fischer, B.F. Habenicht, A.B. Madrid, W.R. Duncan, and O. v. Prezhdo, "Regarding the validity of the time-dependent Kohn–Sham approach for electron-nuclear dynamics via trajectory surface hopping," J Chem Phys **134**(2), 024102 (2011).

[22] J.K. Yu, C. Bannwarth, E.G. Hohenstein, and T.J. Martínez, "Ab Initio Nonadiabatic Molecular Dynamics with Hole-Hole Tamm-Dancoff Approximated Density Functional Theory," J Chem Theory Comput **16**(9), 5499–5511 (2020).

[23] S. Faraji, S. Matsika, and A.I. Krylov, "Calculations of non-adiabatic couplings within equation-of-motion coupled-cluster framework: Theory, implementation, and validation against multi-reference methods," Journal of Chemical Physics **148**(4), 44103 (2018).

[24] P. Nijjar, J. Jankowska, and O. v Prezhdo, "Cite as," Ab Initio Ehrenfest Dynamics The Journal of Chemical Physics **150**, 204124 (2019).

[25] S.A. Fischer, B.F. Habenicht, A.B. Madrid, W.R. Duncan, and O. v. Prezhdo, "Regarding the validity of the time-dependent Kohn–Sham approach for electron-nuclear dynamics via trajectory surface hopping," J Chem Phys **134**(2), 024102 (2011).

[26] C.F. Craig, W.R. Duncan, and O. v Prezhdo, "Trajectory Surface Hopping in the Time-Dependent Kohn-Sham Approach for Electron-Nuclear Dynamics," (2005).

[27] M. T. do Casal, J.M. Toldo, M. Pinheiro Jr, and M. Barbatti, "Fewest switches surface hopping with Baeck-An couplings," Open Research Europe **1**, 49 (2022).

[28] S. Hammes-Schiffer, and J.C. Tully, "Proton transfer in solution: Molecular dynamics with quantum transitions," J Chem Phys **101**(6), 4657 (1998).

[29] I.G. Ryabinkin, J. Nagesh, and A.F. Izmaylov, "Fast Numerical Evaluation of Time-Derivative Nonadiabatic Couplings for Mixed Quantum-Classical Methods," Journal of Physical Chemistry Letters **6**(21), 4200–4203 (2015).

[30] F. Plasser, M. Ruckenbauer, S. Mai, M. Oppel, P. Marquetand, and L. González, "Efficient and Flexible Computation of Many-Electron Wave Function Overlaps," J Chem Theory Comput **12**(3), 1207–1219 (2016).

[31] J.C. Tully, "Molecular dynamics with electronic transitions," J Chem Phys **93**(2), 1061 (1998).

[32] Y. Lin, and A. v. Akimov, "Dependence of Nonadiabatic Couplings with Kohn-Sham Orbitals on the Choice of Density Functional: Pure vs Hybrid," Journal of Physical Chemistry A **120**(45), 9028–9041 (2016).

[33] L. Li, J.C. Wong, and Y. Kanai, "Examining the Effect of Exchange-Correlation Approximations in First-Principles Dynamics Simulation of Interfacial Charge Transfer," J Chem Theory Comput **13**(6), 2634–2641 (2017).

[34] Y. Zhu, and R. Long, "Density Functional Theory Half-Electron Self-Energy Correction for Fast and Accurate Nonadiabatic Molecular Dynamics," Journal of Physical Chemistry Letters **12**(44), 10886–10892 (2021).

[35] W. Li, and A. V Akimov, "How Good Is the Vibronic Hamiltonian Repetition Approach for Long-Time Nonadiabatic Molecular Dynamics?," J. Phys. Chem. Lett **13**, 16 (2022).

[36] N.W. Ashcroft, and D.N. Mermin, *Solid State Physics* (Holt, Rinehart and Winston, 1976).

[37] A. v. Akimov, J.T. Muckerman, and O. v. Prezhdo, "Nonadiabatic dynamics of positive charge during photocatalytic water splitting on GaN(10-10) surface: Charge localization governs splitting efficiency," J Am Chem Soc **135**(23), 8682–8691 (2013).

[38] G. Dutta Pal, B. Dutta, T. Ganguly, and J. Chowdhury, "Role of gold nanocolloids on the photostability of 2-hydroxy-5-methyl benzaldehyde molecule and evidence of excited state intramolecular proton transfer process aided by DFT, non-adiabatic Ab Initio molecular dynamics simulations," J Lumin **188**, 378–387 (2017).

[39] H. Langer, and N.L. Doltsinis, "Nonradiative decay of photoexcited methylated guanine," Physical Chemistry Chemical Physics **6**(10), 2742–2748 (2004).

[40] H. Nieber, and N.L. Doltsinis, "Elucidating ultrafast nonradiative decay of photoexcited uracil in aqueous solution by ab initio molecular dynamics," Chem Phys **347**(1–3), 405–412 (2008).

[41] P.R.L. Markwick, N.L. Doltsinis, and J. Schlitter, "Probing irradiation induced DNA damage mechanisms using excited state Car-Parrinello molecular dynamics," Journal of Chemical Physics **126**(4), (2007).

[42] S.R. Mercier, O. v. Boyarkin, A. Kamariotis, M. Guglielmi, I. Tavernelli, M. Cascella, U. Rothlisberger, and T.R. Rizzo, "Microsolvation effects on the excited-state dynamics of protonated tryptophan," J Am Chem Soc **128**(51), 16938–16943 (2006).

[43] A. v. Akimov, and O. v. Prezhdo, "Nonadiabatic dynamics of charge transfer and singlet fission at the pentacene/C60 interface," J Am Chem Soc **136**(4), 1599–1608 (2014).

[44] T.W. Kim, S. Jun, Y. Ha, R.K. Yadav, A. Kumar, C.Y. Yoo, I. Oh, H.K. Lim, J.W. Shin, R. Ryoo, H. Kim, J. Kim, J.O. Baeg, and H. Ihee, "Ultrafast charge transfer coupled with lattice phonons in two-dimensional covalent organic frameworks," Nature Communications 2019 10:1 **10**(1), 1–10 (2019).

[45] Z. Zhou, J. Liu, R. Long, L. Li, L. Guo, and O. v. Prezhdo, "Control of Charge Carriers Trapping and Relaxation in Hematite by Oxygen Vacancy Charge: Ab Initio Non-adiabatic Molecular Dynamics," J Am Chem Soc **139**(19), 6707–6717 (2017).

[46] B.F. Habenicht, C.F. Craig, and O. v Prezhdo, "Time-Domain Ab Initio Simulation of Electron and Hole Relaxation Dynamics in a Single-Wall Semiconducting Carbon Nanotube," (2006).

[47] B.F. Habenicht, and O. v. Prezhdo, "Time-domain Ab initio study of nonradiative decay in a narrow graphene ribbon," Journal of Physical Chemistry C **113**(32), 14067–14070 (2009).

[48] B.F. Habenicht, and O. v. Prezhdo, "Nonradiative quenching of fluorescence in a semiconducting carbon nanotube: A time-domain Ab initio study," Phys Rev Lett **100**(19), 197402 (2008).

[49] E. Posenitskiy, M. Rapacioli, B. Lepetit, Di. Lemoine, and F. Spiegelman, "Non-adiabatic molecular dynamics investigation of the size dependence of the electronic relaxation in polyacenes," Physical Chemistry Chemical Physics **21**(23), 12139–12149 (2019).

[50] E. Posenitskiy, M. Rapacioli, D. Lemoine, and F. Spiegelman, "Theoretical investigation of the electronic relaxation in highly excited chrysene and tetracene: The effect of armchair vs zigzag edge," Journal of Chemical Physics **152**(7), (2020).

[51] X. Xu, and W.A. Goddard, "The extended Perdew-Burke-Ernzerhof functional with improved accuracy for thermodynamic and electronic properties of molecular systems," J Chem Phys **121**(9), 4068–4082 (2004).

[52] J.P. Perdew, K. Burke, and M. Ernzerhof, "Generalized Gradient Approximation Made Simple," (1996).

[53] S. Goedecker, and M. Teter, "Separable dual-space Gaussian pseudopotentials," Phys Rev B **54**(3), 1703 (1996).

[54] P. Giannozzi, S. Baroni, N. Bonini, M. Calandra, R. Car, C. Cavazzoni, D. Ceresoli, G.L. Chiarotti, M. Cococcioni, I. Dabo, A. Dal Corso, S. de Gironcoli, S. Fabris, G. Fratesi, R. Gebauer, U. Gerstmann, C. Gougoussis, A. Kokalj, M. Lazzeri, L. Martin-Samos, N. Marzari, F. Mauri, R. Mazzarello, S. Paolini, A. Pasquarello, L. Paulatto, C. Sbraccia, S. Scandolo, G. Sclauzero, A.P. Seitsonen, A. Smogunov, P. Umari, and R.M. Wentzcovitch, "QUANTUM ESPRESSO: a modular and open-source software project for quantum simulations of materials," Journal of Physics: Condensed Matter **21**(39), 395502 (2009).

[55] A. v. Akimov, "A Simple Phase Correction Makes a Big Difference in Nonadiabatic Molecular Dynamics," Journal of Physical Chemistry Letters **9**(20), 6096–6102 (2018).

[56] A. v. Akimov, "Libra: An open-Source 'methodology discovery' library for quantum and classical dynamics simulations," J Comput Chem **37**(17), 1626–1649 (2016).

[57] S. V. Kilina, D.S. Kilin, V. V. Prezhdo, and O. V. Prezhdo, "Theoretical study of electron-phonon relaxation in PbSe and CdSe quantum dots: Evidence for phonon memory," Journal of Physical Chemistry C **115**(44), 21641–21651 (2011).

[58] A. V. Akimov, A.J. Neukirch, and O. V. Prezhdo, "Theoretical insights into photoinduced charge transfer and catalysis at oxide interfaces," Chem Rev **113**(6), 4496–4565 (2013).